Journal of Solid State Chemistry 191 (2012) 239–245

Contents lists available at SciVerse ScienceDirect

Journal of Solid State Chemistry

journal homepage: www.elsevier.com/locate/jssc

Porous platinum mesoflowers with enhanced activity for methanol oxidation reaction

Lina Zhuang, Wenjin Wang, Feng Hong, Shengchun Yang*, Hongjun You*, Jixiang Fang, Bingjun Ding

School of Science, MOE Key Laboratory for Non-equilibrium Synthesis and Modulation of Condensed Matter, Xi'an Jiaotong University, Xi'an 710049, People's Republic of China

ARTICLE INFO

Article history:
Received 19 January 2012
Received in revised form
5 March 2012
Accepted 19 March 2012
Available online 27 March 2012

Keywords:
Noble metal
Platinum mesoflower
Methanol oxidation reaction
Porous nanostructure

ABSTRACT

Porous Pt and Pt–Ag alloy mesoflowers (MFs) with about 2 μm in diameter and high porosity were synthesized using Ag mesoflowers as sacrificial template by galvanic reaction. The silver content in Pt–Ag alloys can be facilely controlled by nitric acid treatment. And the pure Pt MFs can be obtained by selective removal of silver element from $Pt_{72}Ag_{28}$ MFs electrochemically. Both $Pt_{45}Ag_{55}$, $Pt_{72}Ag_{28}$ and pure Pt show a high catalytic performance in methanol oxidation reaction (MOR). Especially, pure Pt MFs exhibited a 2 to 3 times current density enhancement in MOR compared with the commercial used Pt black, which can be attributed to their porous nanostructure with 3-dimentional nature and small crystal sizes.

1. Introduction

Direct methanol fuel cells (DMFCs) are promising power sources for portable electronics because of their attractive advantages such as high energy density, low operation temperature, and low pollution for environment [1]. Pt and Pt-based catalysts are known to display the excellent catalytic behavior in DMFCs. However, the expensive nature of platinum is a critical problem and has limited its technological viability. Therefore, it is important that platinum should be used efficiently, with every metal atom functioning during a catalytic process. As a result, Pt nanostructures with high porosity have become promising materials for DMFCs [2].

Recently, various intriguing Pt and Pt-based nanoparticles or nanostructures with different morphologies and high porosity have been successfully synthesized, such as flowerlike, concave, porous, nanodendrites, nanowire network and urchinlike structure [3–7]. Among various nanostructures, the multi-layer and porous mesostructures have attracted intensive research interest because they have high surface area and supply enough adsorption sites for all involved molecules in a narrow space [8–11], leading to the excellent electrocatalytic activity toward methanol oxidation [12]. Therefore, the investigations into the preparation techniques for nanomaterials with multi-layer and porous nanostructure constitute one of major challenges in research today.

Recently, biological molecules have been exploited to synthesize nanoparticles and nanofibers, because they could regulate the unique shapes and the exact sizes of various nanocrystals [13]. Bovine serum albumin (BSA) is one of the most studied proteins, and it has a strong affinity to a variety of inorganic molecules binding to different sites, which makes possible utilization of BSA-decorated nanomaterials in a variety of supramolecular assemblies [14]. Good coverage of silver and gold nanoparticles had been obtained by Ajay and coworkers using BSA as a template because of its zwitterionic character at the protein isoelectric point, which was used to bind to either cationic silver (Ag^+) or anionic gold ($AuCl_4^-$) ions in the foam [15]. These examples indicate that BSA could probably be a promising template for shape-controlled synthesis of noble metal nanoparticles and lead to a special arrangement of noble metal atoms on the nanoparticle surface, making them a better candidate for catalytic applications. However, to our best knowledge, no reports were found to prepare the flower like Ag nanostructures with BAS as soft template.

In this work, we synthesized the Ag mesoflowers (MFs) composed of multi-layer Ag nanosheets with a thickness about 10 nm, using BSA as capping agent and ascorbic acid as reductant. And these 3-dimensional Ag nanostructures were further used as sacrificial template for preparation of Pt nanostructures. In the previous research, most of the products after the galvanic reaction with Ag NPs as template were hollow structures, and the excessive amount of Pt precursor could destroy the final structure of the samples [16,17]. However, in current case, the morphologies of

* Correspondence to: School of Science, MOE Key Laboratory for Non-equilibrium Synthesis and Modulation of Condensed Matter, State Key Laboratory for Mechanical Behavior of Materials, Xi'an Jiaotong University, Xi'an 710049, People's Republic of China. Fax: +86 29 82665995.
E-mail addresses: ysch1209@mail.xjtu.edu.cn (S. Yang), hjyou@mail.xjtu.edu.cn (H. You).

0022-4596/$ - see front matter © 2012 Elsevier Inc. All rights reserved.
http://dx.doi.org/10.1016/j.jssc.2012.03.043

template can be well inherited by the final product, and a novel flower-like Pt and PtAg alloy mesoparticles with porous structure can be prepared. The measurement in electrochemical catalytic performance shows that these prepared Pt MFs exhibit a predominant enhancement in electrocatalytic activity toward electrochemical oxidation of methanol, which can be potentially used to design eletrodes for DMFCs.

2. Experimental details

2.1. Synthesis of Ag mesoflowers (MFs)

Ag MFs were synthesized by reducing $AgNO_3$ (Aldrich, 99+ %) with ascorbic acid in the presence of bovine serum albumin (BSA) working as the template. In a typical synthesis, 0.2 g BSA and 0.169 g $AgNO_3$ were added to 50 mL of deionized water in a 100 mL beaker. The mixture was stirred at room temperature for 30 min until the aqueous solution was transparent. After that, the solution was put in the water-bath with the temperature of 80 °C for 10 min. Then 0.17 g ascorbic acid was added into the solution and the reaction mixture turned light green instantaneously. The mixture was kept at 80 °C for another 10 min and the stirring was maintained through the whole process. The obtained product was collected by centrifugation and washed with water and ethanol to remove most of the BSA. During the washing process, the suspension was centrifuged at 6000 rpm for either 10 or 20 min (depending on whether ethanol or water was used) to remove the excess BSA. Finally, the precipitate was re-dispersed in the deionized water for further use.

2.2. Galvanic replacement reaction

For the synthesis of Pt MFs, chloroplatinic acid was utilized in the galvanic displacement of the Ag MFs. Cleaned Ag MFs (10 mg) were dispersed in water (50 mL) and refluxed under argon in a three-neck round bottom flask (100 mL) equipped with condenser, addition funnel, thermocouple, and stir bar. Upon reaching reflux temperature at 80 °C, chloroplatinic acid (10 mL, 5.0 mM) was added dropwise through the addition funnel over a period of 20 min. The resulting mixture was maintained at the reflux temperature for 20 min until its color became stable and subsequently quenched in an ice bath. After quenching, the product was washed in a saturated sodium chloride (Fisher Scientific) solution to remove the silver chloride precipitate, followed by washing in water and ethanol. Acid treatment was performed in 2 M HNO_3 solution for 60 h and 120 h with stirring, leading to the products of $Pt_{45}Ag_{55}$ and $Pt_{72}Ag_{28}$, respectively.

2.3. Preparation of pure Pt MFs

Pure Pt MFs were obtained after the selective removal of Ag from $Pt_{72}Ag_{28}$ MFs electrochemically because Ag has a much lower standard electrode potential than Pt. In a typical procedure, one milligram of nitric acid-treated $Pt_{72}Ag_{28}$ MFs were dispersed in a mixture of deionized water and isopropanol ($V_{water}/V_{2-isopropanol}=4/1$) at a concentration of 1.0 mg metal catalyst/mL solvent, followed by sonication for 10 min. The final weight percent of metallic catalysts was determined by thermo-gravimetric analysis (TGA) using an STA449C simultaneous TGA/DSC system from NETZSCH Instruments at a ramping rate of 10 °C min^{-1} under an air flow of 50 mL min^{-1}. The mixture was deposited on a glass carbon electrode (3 mm in diameter) and dried under a stream of air. The amount of the metal used in this experiment was 5 μg unless stated otherwise. After evaporation of the water and isopropanol in air, 10 μL of a 0.025 wt% Nafion solution (diluted from 5 wt% Nafion, Ion Power Inc.) was pipeted on the electrode surface in order to attach the catalyst particles onto the glassy carbon and dried in a stream of air, yielding a Nafion® film thickness of ca. 0.1 μm. The electrochemical measurement used a CHI 760 dual channel electrochemical working station (CH instrument, Inc) with a three-electrode system, which consists of a glass carbon electrode with the sample on it, a Pt network counter electrode and a double junction Ag/AgCl reference electrode (Pine, Phychemi Company Limited, 3 M KCl) which have a salt bridge (aqueous KNO_3 solution with a concentration of 10%) between electrode and the solution. The temperature during the measurement was kept at about 25 °C. A 0.1 M perchloric acid ($HClO_4$) aqueous solution was used as the supporting electrolyte in the removal of Ag. The potential for removing silver was monitored based on cyclic voltammetry (CV). Before each experiment, the solution was purged with N_2 for 30 min to remove dissolved oxygen gas. The potential was cycled between −0.2 and 1.1 V for 20 times at a scanning rate of 50 mV s^{-1}.

2.4. Characterization

The morphologies of the Ag, Pt–Ag alloy and pure Pt MFs were characterized using Scanning electron microscopy (SEM) and transmission electron microscopy (TEM). SEM was conducted on a JSM-7000F at 10 KV. TEM samples were prepared by drop casting a dispersion of the MFs onto carbon-coated copper grids. TEM and high-resolution TEM images were acquired using a JEM-2100. X-ray diffraction (XRD) patterns were obtained on a Bruker D8 Advance Diffractometer (Bruker AXS) using a Cu Ka radiation. It's noteworthy that the TEM and SEM sample of pure Pt MFs were prepared by separating the sample from the electrode through ultrasonic process. Typically, after silver dissolution, the electrode was slightly dipped into a glass vial containing 0.5 mL ethanol, while with the ultrasonic treatment, the sample could be separated from the electrode and dispersed in ethanol. The solution was further condensed by evaporating the ethanol in air. And then the dispersion of the MFs was drop casting onto TEM and SEM substrates followed by the UV irradiation for 30 min to remove the Nafion film. The energy dispersive X-ray (EDX) analysis, which was obtained with an Oxford INCA detector installed on the JEOL JSM-7000F instrument, was used to determine the compositions of the samples.

2.5. Electrochemical measurements

All the electrocatalytic samples were prepared in the same way as the $Pt_{72}Ag_{28}$ sample, which was prepared for removing the residual Ag. Electrochemical properties were measured on the same electrochemical workstation described above. The total amount of the metals used in each test was fixed at 5 μg. The commercial used Pt black (JM) was used for comparison. Hydrogen adsorption-desorption cyclic voltammograms (CVs) were recorded in a nitrogen-protected 0.1 M perchloric acid aqueous solution with a scanning rate of 50 mV s^{-1}. The solution was purged by N_2 for 30 min to deplete dissolved O_2. The region for hydrogen adsorption (−0.144–0.206 V on the backward potential scan) was used to estimate the electrochemical active surface areas (EASAs). For methanol oxidation reaction, an air-free aqueous solution containing 0.5 M methanol and 0.1 M perchloric acid was used.

The current densities in cyclic voltammograms and chronoamperograms are evaluated with respect to the electrochemically active Pt area estimated from the hydrogen underpotential deposition charge, assuming that oxidation of a monolayer of H_{UPD} consumes 210 μC cm^{-2} charge. All of the experiments were conducted at room temperature (25 °C).

3. Results and discussions

Fig. 1(a) and (b) illustrates a typical morphology of the as-prepared Ag MFs using BSA as template, which is characterized by a multi-layer structure with the average diameter of about 2 μm. It can be clearly found that the petals on the Ag MFs surface stretching to different directions which have a thickness about 10 nm (Fig. 1(b)). The EDX result shown in the insert of Fig. 1a indicates that the products are exclusively composed of silver. TEM image (Fig. 1(c)) provides more details for this structure, and the clear contrast between the dark center and outer bright regions further indicates that the petals radially grow from the center of the particle. The insert in Fig. 1(c) is the corresponding selected-area electron diffraction (SAED) patterns obtained from one of the petals, revealing they are single-crystalline and can be indexed to face-centered cubic (fcc) Ag. The HRTEM image in Fig. 1(d) provides further insight into its structure. It is observed that the individual petals exhibit good crystalline and highly ordered, continuous fringe patterns. The measured interplane spacing for the lattice fringe is 0.24 nm, which corresponds to the {1 1 1} lattice planes of fcc Ag.

Ag nanoparticles with various morphologies have been widely used as sacrifical template to synthesize other noble metal particles such as Au, Pt and Pd, with hollow and porous structures [16–19]. Since the standard reduction potential of $PtCl_6^{2-}$/Pt pair (0.73 V vs standard hydrogen electrode, SHE) is higher than that of the Ag^+/Ag pair (0.80 V vs SHE), silver would be oxidized into Ag^+ when silver nanostructures and H_2PtCl_6 are mixed in an aqueous solution:

$$4Ag(s)+PtCl_6^{2-}\rightarrow Pt(0)+4Ag^+_{(aq)}+6Cl^-_{(aq)} \quad (1)$$

$$Pt(0)+Ag\ (0)\rightarrow PtAg\ (alloy) \quad (2)$$

In current case, Pt–Ag alloy and pure Pt mesoflowers were well prepared by using the as-prepared Ag MFs as template. As one can see from the SEM images in Fig. 2(a) and (d), the resulting products was still keep a morphology similar with that of Ag MFs. As we have described in experimental part, Pt–Ag alloy MFs with different atomic ratios can be syntheiszed by acid treatment of the products for 60 h and 120 h after galvanic reaction, which can be detected by EDX analysis. As shown in Fig. 2(b) and (e), the EDX results shows that the acid treatment performed in 2 M HNO_3 solution for 60 h and 120 h leading to the products with atomic ratios between Pt and Ag were 1:1.2 and 26:1, from which the samples can be defined as $Pt_{45}Ag_{55}$ and $Pt_{72}Ag_{28}$, respectively. The representative TEM images (Fig. 2(c) and (g)) of single $Pt_{45}Ag_{55}$ and $Pt_{72}Ag_{28}$ alloy MFs show a similar profile with that of Ag MFs in which the petals stretch out from the center. However, compared with the silver MFs, the alloy MFs shows a broadening of SAED spots, especially for that of the high-index crystal planes, suggest a common orientation with a small angle lattice mismatch between the primary NP building units. The HRTEM images shown in Fig. 2(d) and (h) recorded from the cycled area in Fig. 2(c) and (g) further support this suggestion. As typically indicated by the black lines in Fig. 2(h), the lattice orientation of two attached grains has a misorientation less than 5°. Meanwhile, the HRTEM studies reveal that the petals of alloy MFs are porous structure and composed of nanoparticles with diameter less than 5 nm, as labeled by the arrows and dashed lines in Fig. 2(d).

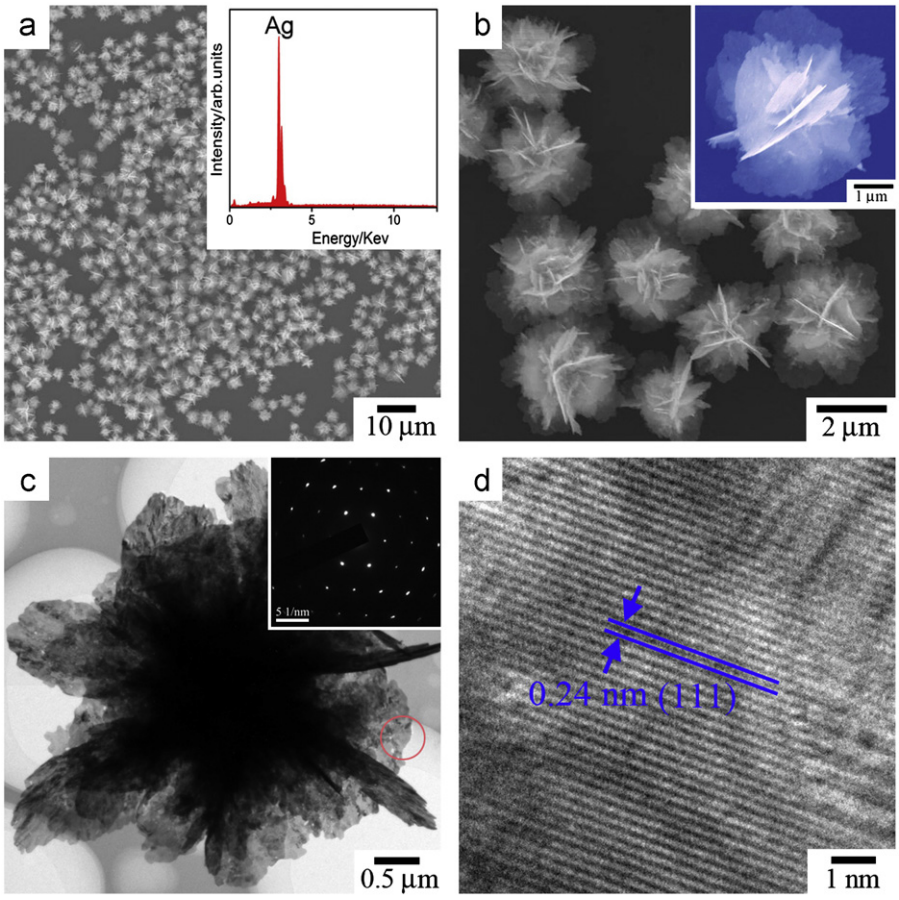

Fig. 1. (a) Overview SEM image of the Ag MFs, the inset showing the corresponding EDX pattern; (b) enlarged SEM image of several Ag MFs with uniform size; (c) TEM image of a single Ag MF, the inset is the corresponding SAED pattern; (d) HRTEM image of the thin layer in Ag MF. The silicon signals came from the silicon substrate on which the sample is supported.

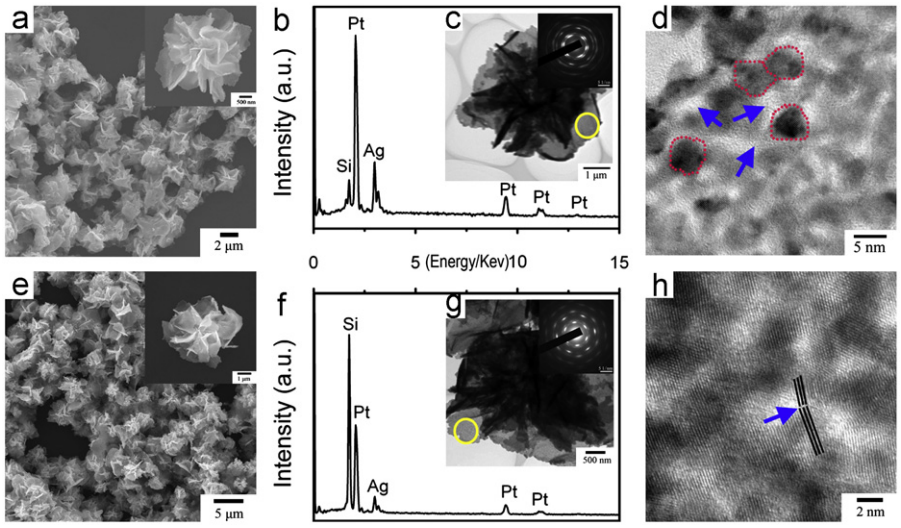

Fig. 2. Representative (a) SEM, (b) TEM and (c) HRTEM images of $Pt_{45}Ag_{55}$; (d) SEM, (e) TEM and (f) HRTEM images of $Pt_{72}Ag_{28}$. The insets in (a) and (d) are the enlarged SEM images for $Pt_{45}Ag_{55}$ and $Pt_{72}Ag_{28}$, respectively. The insets in (b) and (e) are the corresponding SAED patterns.

It was hard to remove silver element from the alloys completely. Our additional experiment reveals that there were still 18% (in weight) Ag remained even after immersing in 2 M nitric acid for 5 day. This phenomenon may be due to the formation of Pt–Ag solid solution during the galvanic reaction occurring between metallic silver and Pt (IV) ions, which leads to the dissolution of Ag in nitric acid difficult. Therefore, in order to completely remove the residual Ag from Pt–Ag alloy MFs, the electrochemical method was employed, as described in experimental part. As shown in Fig. 3, the peak located at around 1.0 V (vs. Ag/AgCl) can be ascribed to the silver electro-oxidation reaction presented a continuous decrease during the CV cycling, which nearly disappeared after 10 CV cycles, indicating the silver was removed from the electrode after the CV cycling through follow Eq. (3) [20].

$$Ag(s) + e \rightarrow Ag^{+}_{(aq)} \quad (3)$$

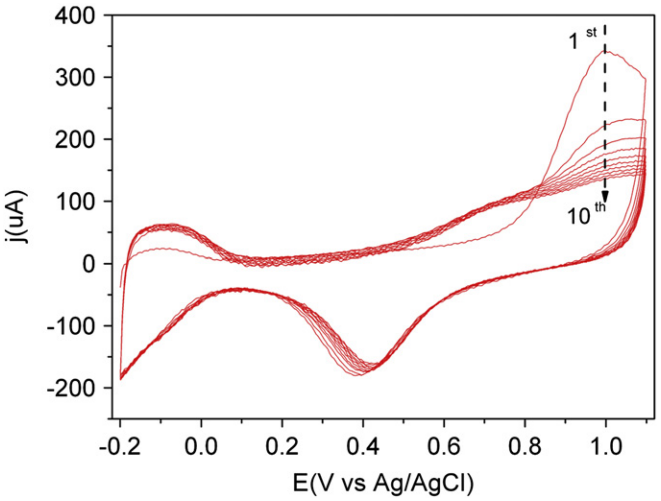

Fig. 3. CV curves of ten continuous cycles for Ag dissolution from $Pt_{72}Ag_{28}$ MFs with a scan range between −0.2 and 1.1 V in 0.1 M $HClO_4$ solution at room temperature.

The SEM images of the final products were displayed in Fig. 4(a) and (b), indicating that the morphology of the mother Ag MFs shape were kept very well after the galvanic reactions and electrochemical dissolution of Ag from PtAg alloys. Further EDX analysis (inset in Fig. 4(a)) was used to determine the elemental compositions for the final products. The result shows that no silver signals can be detected, indicating the final product is exclusively composed of platinum. SAED pattern in Fig. 4(d) indicates that Pt MF structure is polycrystalline in nature with certain degrees of preferential orientation, which is similar with that of their alloy counterparts. TEM images (Fig. 4(c)–(e)) provide more details for this structure that each sheet on the Pt MFs consists of a three-dimensinal continuous nanoporous structure with a pore size around 2 nm (Fig. 4(e)). The pores uniformly dispersed on above petals are smaller and denser than those (~5 nm) shown in the porous metals prepared through galvanic reaction or dealloy treatment reported by others [16–19]. A large number of crystal defects can be observed in the HRTEM image, as marked in Fig. 4(f) by black arrows, which may potentially act as the active site during the catalysis.

XRD was further used to analyze the crystalline structure of Ag, Pt and Pt–Ag samples, respectively. As shown in Fig. 5, both four kinds of samples show diffractions that could be indexed to (1 1 1), (2 0 0), (2 2 0), (3 1 1) and (2 2 2) planes of a fcc lattice. No other diffraction peak was observed, indicating these products were phase pure. The observed diffraction angles for both $Pt_{45}Ag_{55}$ and $Pt_{72}Ag_{28}$ nanostructures fell between those of the two pure metals and the diffraction peak positions of alloy samples linearly shifted and moved to high angles with the decrease of Ag/Pt ratio (dashed lines in Fig. 5), suggesting the formation of alloy nanoparticles [21]. It is well known that Ag–Pt bimetallics have a large miscibility gap at the temperature below about 1190 °C in bulk [22], and they form alloys only at very high atomic content of either Ag or Pt [23]. However, both theoretical studies and experimental data have shown that the small-size-effect can greatly promote the miscibility between the metal elements with the decrease in particle size [21,24–27]. In current case, as labeled in Fig. 2(d), the average cluster sizes were about 5 nm, which was much smaller than the threshold value of the size (20 nm) of alloying nanoparticles for the unusual solid solubility [26]. Therefore, with the progress of reaction, platinum ions became reduced to metal leading to the formation of Pt–Ag solid solution with the residual silver.

One potentially very important application area of such 3-dimentional Pt nanostructures is to prepare the fuel cell

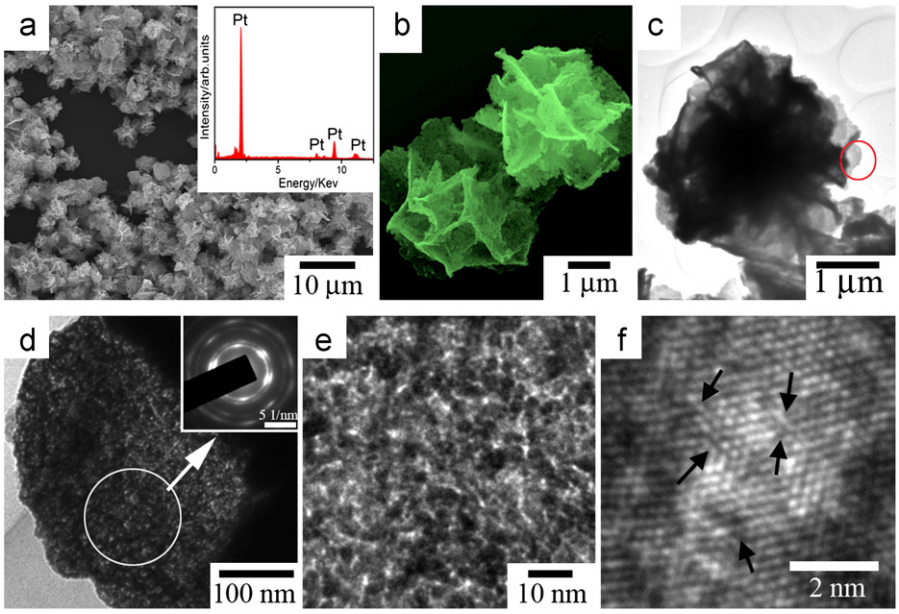

Fig. 4. SEM images of Pt MFs at low magnification (a) and high magnification (b), the inset in (a) showing the corresponding EDX pattern; TEM image of a single Pt MFs (c) and a single layer of the MF (d), the inset shows the corresponding SAED pattern (the circled part); (e) and (f) show the enlarged TEM and HRTEM images of the circled part in Fig. 2(d).

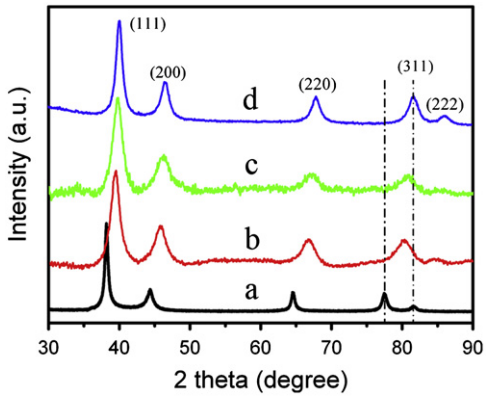

Fig. 5. The XRD patterns for Ag (a), $Pt_{45}Ag_{55}$ (b), $Pt_{72}Ag_{28}$ (c) and Pt (d) MFs.

electrode. Herein, the electrochemical catalytic activity in methanol oxidation was examined, as this reaction was sensitive to the surface electronic structure and atomic arrangement of Pt [28,29]. The ECSAs of the Pt and Pt–Ag MFs were calculated by measuring the hydrogen adsorption on Pt (Fig. 6(a)). The ECSAs for $Pt_{45}Ag_{55}$, $Pt_{72}Ag_{28}$, Pt MFs and Pt black (JM) were 10.3, 14.1, 13.9 and 12.96 $m^2\ g^{-1}$, respectively. The ECSAs of $Pt_{72}Ag_{28}$ and Pt MFs were comparable to that of Pt black, which should be due to that Pt or PtAg MFs were composed by the cluster with an average size less than 5 nm, while the crystal size in Pt black was ranging from 5–10 nm (Fig. S1 in supplemental data).

The cyclic voltametric (CV) measurements of methanol oxidation were carried out in solution of 0.1 M $HClO_4$+0.5 M CH_3OH at room temperature at a scan rate of 50 mV s^{-1} (Fig. 6(b) and (c)), from which we observed that the onset potential at first anodic scanning for methanol oxidation is about 0.38 V, 0.37 V, 0.39 V and 0.40 V for $Pt_{45}Ag_{55}$, $Pt_{72}Ag_{28}$, pure Pt MFs and Pt black, respectively, indicating that both pure Pt–Ag and Pt MFs have an enhancement in the kinetics of methanol oxidation reaction compared with the Pt black. Herein the onset potential being defined as the potential at which 10% of the current value at the peak potential was reached [30]. More importantly, as shown in Fig. 6(d), the specific area and mass current densities of the pure Pt MFs sample are of 3.42 mA cm^{-2} and 455 mA mg^{-1}, respectively, about 2 to 3 times higher than the values of Pt black 1.81 mA cm^{-2} and 157 mA mg^{-1}, respectively. And such values were also higher than that of porous Pt nanotubes in specific area value (1.62 mA cm^{-2}) [31] and the porous single-crystalline Pt nanoparticles in mass current density (205 mA mg^{-1}) [12]. This fact indicates the pure Pt MFs exhibit much improved performance toward MOR.

The peaks of methanol oxidation with high current density are clearly observed at around 0.7 V (vs. Ag/AgCl) in anodic sweep and at around 0.55 V (vs. Ag/AgCl) in cathodic sweep. Generally, as described by others, the following conventional elementary reaction processes are considered [32–34]:

$$Pt + CH_3OH \rightarrow Pt\text{–}CO + 4H^+ + 4e^- \quad (4)$$

$$Pt + H_2O \rightarrow Pt\text{–}OH + H^+ + e^- \quad (5)$$

$$Pt\text{–}CO + Pt\text{–}OH \rightarrow 2Pt + CO_2 + H^+ + e^- \quad (6)$$

While the total electrooxidation of methanol is expressed as:

$$CH_3OH + H_2O \rightarrow CO_2 + 6H + 6e^- \quad (7)$$

First, when the potential arrives at around 0.50 V in the anodic sweep, methanol molecule adsorbs on the Pt surface and generates Pt–CO (Eq. (4)). Meanwhile, water molecule oxidation produces Pt–OH at more anodic potential, as illustrated by Eq. (5). With the increase of potential, the adsorption and oxidation will be enhanced gradually, which lead to a continuous increase in current density until the potential reaches to around 0.7 V, as shown in Fig. 6(b). As the potential increases, more and more reaction products will prevent the deeper oxidation. As a result, the peak will then decrease. Under this potential region, the redox of two adsorbed species will produce Pt and CO_2 for desorption (Eq. (6)). While when the potential arrives at around 0.65 V in the cathodic sweep, methanol reoxidation is generated again and the peak climbs to a new high value of around 0.55 V.

The ratio between the forward (I_f) and reverse (I_b) anodic peak current densities, I_f/I_b, has been used to describe the tolerance of a

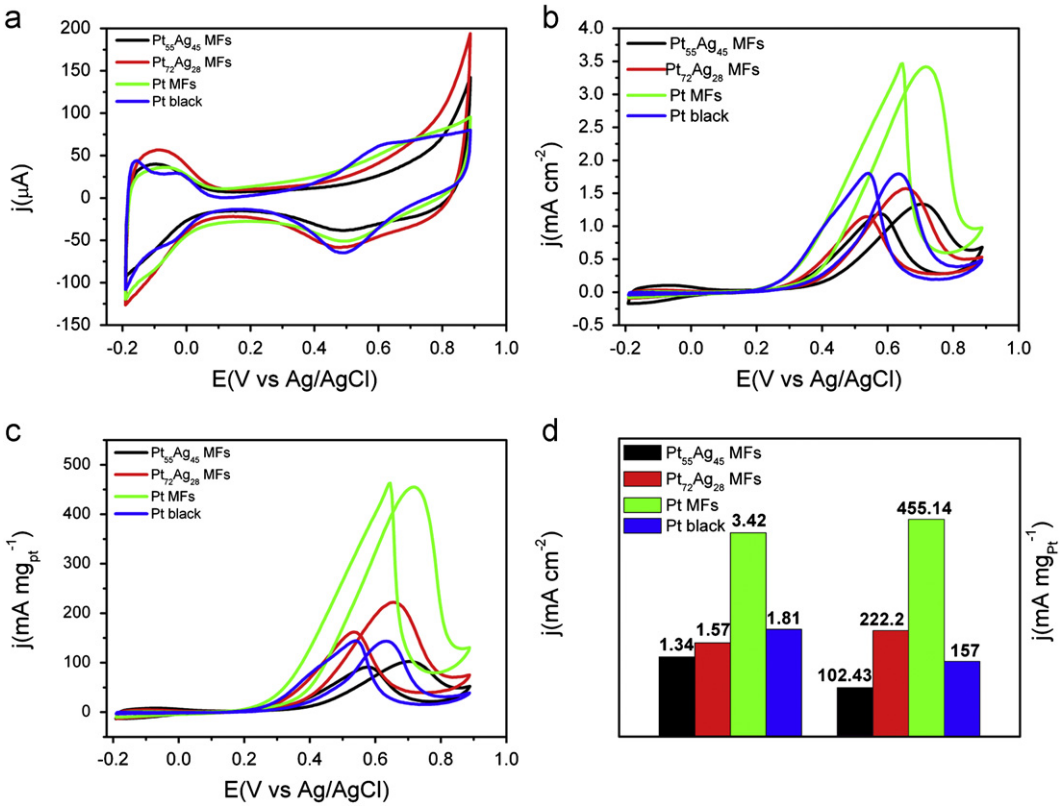

Fig. 6. (a) CV profiles of Pt and Pt–Ag MFs in 0.1 M $HClO_4$ solution at room temperature; (b) and (c) CVs of MOR on Pt and Pt–Ag MFs catalysts in 0.1 M $HClO_4$ and 0.5 M CH_3OH for specific area current and specific mass current, respectively; (d) Comparison of peak specific area current and peak specific mass current of Pt MFs, Pt–Ag MFs and Pt black. All the scanning rate was 50 mv s^{-1}.

catalyst to the accumulation of carbonaceous species [35–40]. Low I_f/I_b ratio is an indication of poor oxidation of methanol to carbon dioxide during an anodic scan and accumulation of carbonaceous residues on the catalyst surface. Catalyst with low I_f/I_b ratio is prompt to extended CO poisoning [41,42], while a higher ratio indicates more effective removal of the poisoning species on the catalyst surface [39]. The I_f/I_b ratios calculated from the CV curves for $Pt_{45}Ag_{55}$, $Pt_{72}Ag_{28}$, pure Pt MFs and Pt black were 1.13, 1.36, 0.988 and 0.982, respectively. It appears that although the remained Ag produces a negative effect on anodic scanning current density, the Pt–Ag alloys presents a better CO tolerance than pure Pt catalyst. This result was also proved by He and Peng in their recent works [20,43].

As reported by others, the porous substrate, such as highly ordered mesoporous carbon, can significantly improve the specific activity of platinum-based catalysts because of the facile transport of methanol and the oxidation products in the pores [44–45]. In current case, The noteworthy electrochemical catalytic performance of Pt MFs can be attributed to their unique 3-dimensional architecture, where the interconnected interstices and channels extending in all three dimensions allow the rapid diffusion and mass transport of external reagents directly to the surface of Pt catalysts, as well as unblocked transport of electrons, which contributes greatly to the enhancement of catalytic properties [46–56]. As for the Pt–Ag alloys, it is well known that methanol electrooxidation occurs preferentially on electrode surfaces with continuous neighboring Pt sites [50]. Therefore, when the Ag content is higher in the Pt–Ag MFs, a number of Pt atoms will exist in the form of monomers (single atoms), dimers, or clusters of Pt atoms which do not provide effective dissociative adsorption of methanol molecules [51]. Meanwhile, Ag atom itself is much less active to MOR in acidic

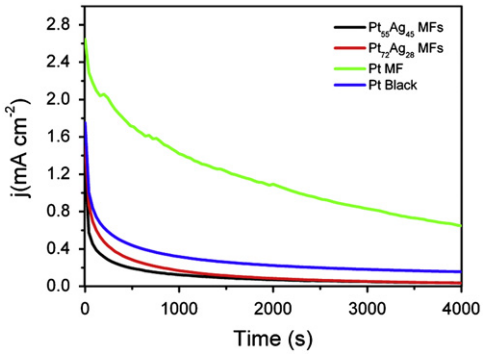

Fig. 7. Chronoamperometric response of oxidation of 0.5 M methanol in 0.1 M $HClO_4$ solution under a constant potential of 0.65 V (vs. Ag/AgCl).

conditions, so the decline of activity can be correlated to the accumulation of more Ag atoms on the surface [20]. Therefore, after electrochemically removing Ag atoms, the pure Pt MFs exhibit distinct enhancement for MOR. However, the improved performance in tolerating poisoning species for Pt–Ag alloy, especially for $Pt_{78}Ag_{22}$ may be due to the electronic structure of Pt being changed by forming alloy with Ag [38], but the mechanism was still not clear yet, which need to be further investigated.

The long-term performance of Pt and Pt–Ag MFs catalysts compared with commercial used Pt black (TKK) was evaluated by chronoamperometric measurement under a constant potential of 0.65 V versus Ag/AgCl for 4000 s, as shown in Fig. 7. The polarization currents of all the present catalysts decrease rapidly at the initial stage. This may be due to the formation of intermediate species, such as CO_{ads}, $COOH_{ads}$, and CHO_{ads}, during the methanol oxidation reaction [52–54]. And the following

degradation in the current can be attributed to the accumulation of CO_{ads} poisioning species on the surface of Pt electrode during the MOR process [55,56]. Pt MFs produced an initial specific activity of 2.65 mA cm^{-2} and a final specific activity of 0.65 mA cm^{-2}, indicating a 24.5% activity left after 4000 s. In comparison, Pt black produced an initial specific asctivity of 1.75 mA cm^{-2} and a final specific activity of 0.15 mA cm^{-2}, indicating the lost activity was more than 92%. Similar with the observations from Fig. 6, the samples of $Pt_{45}Ag_{55}$ and $Pt_{72}Ag_{28}$, show a much low steady-state current density, which indicates that the PtAg alloys have a less activity toward methanol oxidation compared with pure Pt catalysts.

4. Conclusion

In summary, we synthesized 3-D Ag MFs using BSA as capping agent, which can be further used as sacrificial template for the preparation of porous Pt and Pt–Ag alloy nano-catalysts. The morphology of Ag MFs can be kept very well by their Pt and Pt–Ag alloy counterpart. The produced Pt and PtAg alloy MFs shows higher electrocatalytic activities and catalyst tolerance that can be applied in DMFCs in comparison with the commercial used Pt black in methanol electro-oxidation. The current study provided a facile approach for the development of high performance Pt or other noble metals and their alloy-based electrocatalysts for fuel cells or electrochemical sensors.

Acknowledgment

This work was supported by the National Natural Science Foundation of China (No. 50901056), Doctoral Fund for New Teachers (No.20090201120053) and the Fundamental Research Funds for the Central Universities. J.X.F. is supported by Tengfei Talent Project of Xi'an Jiaotong University.

Appendix A. Supporting information

Supplementary data associated with this article can be found in the online version at http://dx.doi.org/10.1016/j.jssc.2012.03.043.

References

[1] W. Vielstich, A. Lamm, H.A. Gasteiger, Handbook of Fuel Cells: Fundamentals, Technology, Applications, Volume 2: "Fuel Cell Electrocatalysis", John Wiley & Sons, New York, 2003.
[2] G.A. Somorjai, Introduction to Surface Chemistry and Catalysis, John Wiley & Sons, New York, 1994.
[3] S.H. Sun, D.Q. Yang, D. Villers, G.X. Zhang, E. Sacher, J.P. Dodelet, Adv. Mater. 20 (2008) 571–574.
[4] H. Zhang, M.S. Jin, J.G. Wang, W.Y. Li, P.H.C. Camargo, M.J. Kim, D. Yang, Z.X. Xie, Y.N. Xia, J. Am. Chem. Soc. 133 (2011) 6078–6089.
[5] B. Lim, M.J. Jiang, P.H.C. Camargo, E.C. Cho, J. Tao, X.M. Lu, Y.M. Zhu, Y.N. Xia, Science 324 (2009) 1302–1305.
[6] Y.J. Song, R.M. Garcia, R.M. Dorin, H.R. Wang, Y. Qiu, E.N. Coker, W.A. Steen, J.E. Miller, J.A. Shelnutt, Nano Lett. 12 (2007) 3650–3655.
[7] L. Wang, S.J. Guo, J.F. Zhai, S.J. Dong, J. Phys. Chem. C 112 (2008) 13372–13377.
[8] Y.B. He, G.R. Li, Z.L. Wang, Y.N. Ou, Y.X. Tong, J. Phys. Chem. C 114 (2010) 19175–19181.
[9] Jitendra N. Tiwari, Rajanish N. Tiwari, Kwang S. Kima, Prog. Mater. Sci. 57 (2012) 724–803.
[10] Jitendra N. Tiwari, Rajanish N. Tiwari, Gyan Singh, Kun-Lin Lin, Plasmonics 6 (2011) 67–73.
[11] Jitendra N. Tiwari, Rajanish N. Tiwari, Kun-Lin Lin, ACS Appl. Mater. Interfaces 2 (2010) 2231–2237.
[12] M. Nogami, R. Koike, R. Jalem, G. Kawamura, Y. Yang, Y. Sasaki, J. Phys. Chem. Lett. 1 (2010) 568–571.
[13] A.X. Yin, X.Q. Min, Y.W. Zhang, C.H. Yan, J. Am. Chem. Soc. 133 (2011) 3816–3819.
[14] L. Yang, R.M. Xing, Q.M. Shen, K. Jiang, F. Ye, J.Y. Wang, Q.S. Ren, J. Phys. Chem. B 110 (2006) 10534–10539.
[15] A.V. Singh, B.M. Bandgar, M. Kasture, B.L.V. Prasad, M. Sastry, J. Mater. Chem. 15 (2005) 5115–5121.
[16] X.M. Lu, L. Au, J. McLellan, Z.Y. Li, M. Marquez, Y.N. Xia, Nano Lett. 7 (2007) 1764–1769.
[17] Y.G. Sun, Y.N. Xia, J. Am. Chem. Soc. 126 (2004) 3892–3901.
[18] C.X. Xu, R.Y. Wang, M.W. Chen, Y. Zhang, Y. Ding, Phys. Chem. Chem. Phys. 12 (2010) 239–246.
[19] Y.G. Sun, Y.N. Xia, Science 298 (2002) 2176–2179.
[20] Z.M. Peng, H.J. You, H. Yang, Adv. Funct. Mater. 20 (2010) 3734–3741.
[21] Z.M. Peng, H. Yang, J. Solid State Chem. 181 (2008) 1546–1551.
[22] T.B. Massalski, J.L. Murray, L.H. Bennett, H. Baker, Binary Alloy Phase Diagrams, American Society for Metals, Metals Park, OH, 1986.
[23] F.N. Rhines, Phase Diagrams in Metallurgy: Their Development and Application, McGraw-Hill, New York, 1956.
[24] A.S. Shirinyan, M. Wautelet, Mater. Sci. Eng. C-Biomimetic Supramol. Syst. 26 (2006) 735.
[25] A.S. Shirinyan, A.M. Gusak, M. Wautelet, Acta Mater. 53 (2005) 5025.
[26] G. Ouyang, X. Tan, C.X. Wang, G.W. Yang, Nanotechnology 17 (2006) 4257.
[27] M. Wautelet, J.P. Dauchot, M. Hecq, Nanotechnology 11 (2000) 6.
[28] A. Hamnett, Catal. Today 38 (1997) 445–457.
[29] S.W. Lee, S. Chen, W.C. Sheng, N. Yabuuchi, Y.T. Kim, T. Mitani, E. Vescovo, Y. Shao-Horn, J. Am. Chem. Soc. 131 (2009) 15669–15677.
[30] F. Maillard, A. Bonnefont, M. Chatenet, L. Guetaz, B. Doisneau-Cottignies, H. Roussel, U. Stimming, Electrochim. Acta 53 (2007) 811–822.
[31] S.M. Alia, G. Zhang, D. Kisailus, D.S. Li, S. Gu, K. Jensen, Y.S. Yan, Adv. Funct. Mater. 20 (2010) 3742–3746.
[32] J.J. Niu, J.N. Wang, Electrochim. Acta 53 (2008) 8058–8063.
[33] M. Umeda, M. Kokubo, M. Mohamedi, I. Uchida, Electrochim. Acta 48 (2003) 1367–1374.
[34] C. Lamy, J.-M. Leger, in: A. Wieckowski (Ed.), Interfacial Electrochemistry, Marcel Dekker, New York, 1999. (Chapter 48).
[35] Carlo M. Orofeo, Hiroki Ago, Baoshan Hu, Masaharu Tsuji, Nano Res. 4 (2011) 541–549.
[36] Jitendra N. Tiwari Dr., Rajanish N. Tiwari, Yun-Min Chang, Kun-Lin Lin Dr., Chem. Sus Chem. 3 (2010) 460–466.
[37] Jitendra N. Tiwari, Fu-Ming Pan, Rajanish N. Tiwari, S.K. Nandi, Chem. Commun. 48 (2008) 6516–6518.
[38] Jitendra N. Tiwari, Fu-Ming Pan, Kun-Lin Lin, New J. Chem. 33 (2009) 1482–1485.
[39] T.C. Deivaraj, J.Y. Lee, J. Power Sources 142 (2005) 43–49.
[40] S.J. Guo, S.J. Dong, E.K. Wang, Acs Nano 4 (2010) 547–555.
[41] F. Sen, G. Gokagac, J. Phys. Chem. C 111 (2007) 1467–1473.
[42] Z.L. Liu, X.Y. Ling, X.D. Su, J.Y. Lee, J. Phys. Chem. B 108 (2004) 8234–8240.
[43] W.W. He, X.C. Wu, J.B. Liu, K. Zhang, W.G. Chu, L.L. Feng, X.N. Hu, W.Y. Zhou, S.S. Xie, J. Phys. Chem. C 113 (2009) 10505–10510.
[44] F.B. Su, J.H. Zeng, X.Y. Bao, Y.S. Yu, J.Y. Lee, X.S. Zhao, Chem. Mater. 17 (2005) 3960–3967.
[45] G.S. Chai, I.S. Shin, J.S. Yu, Adv. Mater. 16 (2004) 2057–2061.
[46] C.X. Xu, L. Wang, X.L. Mu, Y. Ding, Langmuir 26 (2010) 7437–7443.
[47] C.X. Xu, L.Q. Wang, R.Y. Wang, K. Wang, Y. Zhang, F. Tian, Y. Ding, Adv. Mater. 21 (2009) 2165–2169.
[48] M.L. Anderson, R.M. Stroud, D.R. Rolison, Nano Lett. 2 (2002) 235–240.
[49] S.H. Yoo, S. Park, Adv. Mater. 19 (2007) 1612–1615.
[50] T. Iwasita, Electrochim. Acta 47 (2002) 3663–3674.
[51] B.C. Du, Y.Y. Tong, J. Phys. Chem. B 109 (2005) 17775–17780.
[52] Y.L. Hsin, K.C. Hwang, C.T.J. Yeh, Am. Chem. Soc. 129 (2007) 9999–10010.
[53] Y.J. Gu, W.T. Wong, Langmuir 22 (2006) 11447–11452.
[54] L.H. Jiang, G.Q. Sun, X.S. Zhao, Z.H. Zhou, S.Y. Yan, S.H. Tang, G.X. Wang, B. Zhou, Q. Xin, Electrochim. Acta 50 (2005) 2371–2376.
[55] J. Prabhuram, T.S. Zhao, Z.K. Tang, R. Chen, Z.X. Liang, J. Phys. Chem. B 110 (2006) 5245–5252.
[56] A. Kabbabi, R. Faure, R. Durand, B. Beden, F. Hahn, J.M. Leger, C. Lamy, J. Electroanal. Chem. 444 (1998) 41–53.